SUB-RESOLUTION SURFACE PROPERTIES OF COMET 67P/CHURYUMOV-GERASIMENKO FROM HAPKE MODELING AND IMPLICATIONS FOR MATERIAL TRANPORT. S.A. Moruzzi[1,2], A.G. Hayes[1], P. Corlies[3], J.M. Soderblom[3], S.P.D. Birch[3], N.W. Kutsop[1], [1]Cornell University, Ithaca, NY [2]University of Arizona, Tucson, AZ (smoruzzi@email.arizona.edu) [3]MIT, Cambridge, MA

Introduction: Comets consist of volatiles and other primitive material from the solar system's formation. Understanding the active and erosional processes shaping their surfaces is key to using them to gain insights into presolar history, the initial stages of planet formation, and the materials delivered to early Earth. Observations of comet 67P/Churyumov Gerasimenko (67P) from the Rosetta spacecraft's Optical, Spectroscopic, and Infrared Imaging System (OSIRIS) Narrow Angle Camera (NAC) have provided meter-scale images of a cometary surface, revealing that it is dominated by distinct morphologic classes including smooth plains, cauliflower plains, pitted plain, and consolidated terrains [1–3]. To quantitatively define these terrains as stages of surface evolution, we derive multispectral phase curves for type-examples of each primary morphologic unit both pre- and post-perihelion. We then fit the curves to Hapke, (2012) photometric functions [4]. Best-fitting photometric properties, such as single scattering albedo and macroscopic roughness, are compared to previously published best-fit Hapke coefficients of disk-integrated reflectance [5,6], and used to interpret surface properties for each morphologic unit.

Our results are consistent with the qualitative interpretation that the smooth plains are the smoothest of the four terrains and exhibit the highest albedo, and the consolidated terrains are the roughest terrains and exhibit the lowest albedo. Comparisons to disk-integrated values show that the comet (at the time of the disk-integrated observations [6]) primarily showed cauliflower plains to the spacecraft. We find that the variations in spectral slope between pre- and post- perihelion fits are independent of morphology and comet latitude while the spectral slopes themselves do change from unit to unit, suggesting processes act both globally and locally.

Methods: Rosetta's OSIRIS NAC images, taken in wavelengths ranging from ~200–1000 nm, revealed a diverse and evolving landscape across the surface of the comet, showing two broad terrain categories: smooth terrains and rough terrains [1]. Smooth terrains consist of small, granular material that is hypothesized to have been previously consolidated bedrock. These terrains include smooth, pitted, and cauliflower plains. In contrast, consolidated terrains (low reflectance [5,7]) consist of the exposed comet nuclei, or bedrock, including cliff terrains [1].

We have chosen four morphologies, as defined by [1], from which to select example regions for this study. A total of 15 sites across the comet's surface were chosen: seven are examples of smooth plains, four are examples of pitted plains, two are examples of cauliflower plains and two are examples of consolidated terrains. We use the SPICE toolkit from NAIF [7] to generate navigation information for each pixel and determine the relevant incidence, emission, and phase angles. For each of the selected sites, we chose a representative image and manually selected a region of interest.

We utilized the reflectance function from [4] that includes macroscopic roughness and similar methodology to [6] to fit our phase curves and in doing so, determine our best fit "Hapke parameters": single scattering albedo (ω), an asymmetry parameter for the Henyey-Greenstein Function (ξ), the coefficient of the shadow-hiding opposition effect function (B_{S0}), internal parameter shadow hiding opposition effect function parameter (h_s) and macroscopic roughness (θ). We use a Levenberg-Marquardt curve fitting routine and 1000-run Monte Carlo simulations to search within specified ranges of these parameters for the best fit values for the observed phase curves. An empirical correction accounting for interfacet multiple scattering was employed but had a minor effect on our results [4]. To minimize the correlation between albedo and roughness, 480 nm, 535 nm, 649 nm and 882 nm filters were fit simultaneously, allowing for variations in single scattering albedo and asymmetry parameters with wavelength, but not in BS_0, h_s or macroscopic roughness. Pre-perihelion and post-perihelion data were analyzed separately.

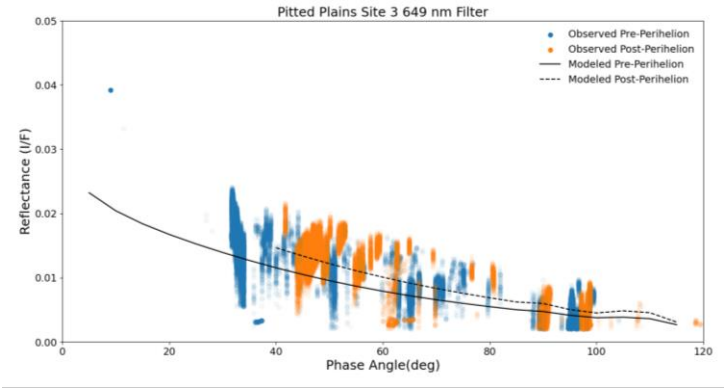

Figure 1: **Observed and modeled phase curves for pre- and post-perihelion for an example morphology and site (pitted plains site 3) in the 649 nm filter.**

Photometric Results: Both the observed and modeled phase curves for the smooth plains have a steep slope and the highest I/F values at low phase,. The slope of the curves decrease as for the consolidated terrains (Fig. 1). The consolidated terrains as well as some example sites for the other morphologies lack low phase angle observations, so we are unable to constrain B_{S0} and h_s. In these cases, we do not include these parameter in our fits.

Comparison to results from [6] show that our albedo values for all morphologies, filters, and temporal divisions are greater than the disk-integrated values. For cauliflower plains, our derived albedos pre- and post-perihelion are the closest to the disk-integrated [6] albedo parameters for all filters. This analysis may suggest that the photometric behavior of the cauliflower plains contributes the most to the disk-integrated photometric values.

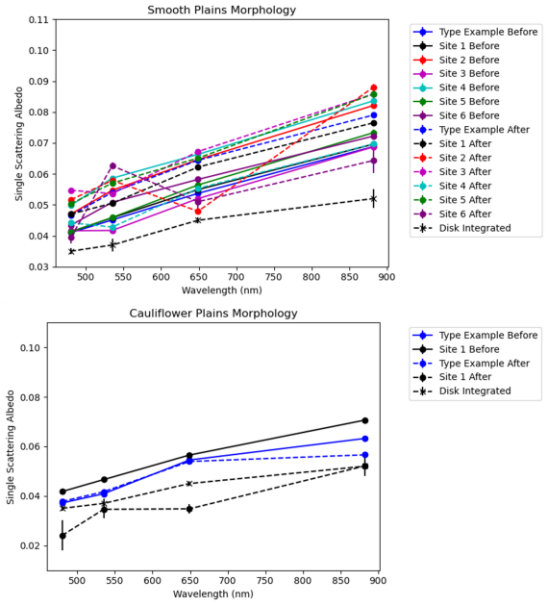

Figure 2: **Wavelength Dependence curves of best-fit single scattering albedo for all studied examples of smooth plains and cauliflower plains morphologies and disk-integrated.**

We also explored trends across wavelengths within each morphology, site and temporal division. We see a generally increasing trend of single scattering albedo with wavelength (Fig. 2) for all sites pre- and post-perihelion, though the temporal differences in magnitudes of single scattering albedo wavelength curves depend on the site. There is no distinguishable trend for the asymmetry parameter across wavelengths.

Material Transport: We compute spectral slopes for each site pre- and post- perihelion using the best fit single scattering albedos at 882 and 649 nm. Temporal differences in spectral slope suggest spectral reddening or bluing depending on the site in question. An increase in spectral slope post-perihelion suggests a spectral reddening, usually associated with loss of surface water ice or burial by depleted material, while a decrease in spectral slope post-perihelion suggests a spectral bluing, usually associated with the exposure of water ice-rich material [6,8]. For example, in the smooth plains morphology, we see spectral reddening for sites 2 and 5 (Fig 3), spectral bluing for the type-example and site 1, and no spectral change within error for sites 3, 4 and 6. There is similar variation in spectral slope of the example sites for the other three morphologies.

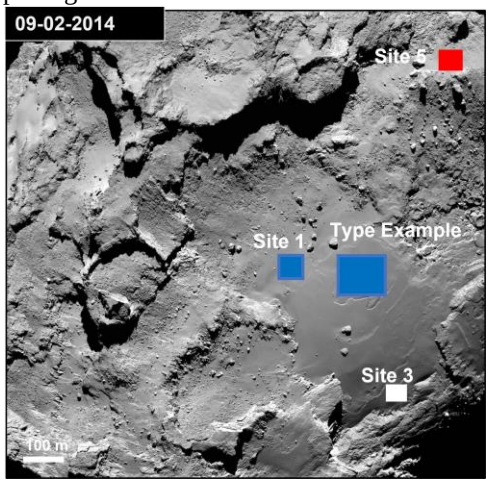

Figure 3**: Spectral changes between pre- and post- perihelion for example sites of the smooth plains morphology. Regions of interest are in color, where blue indicated a decrease in brightness post-perihelion, red indicates an increase in brightness, and white indicates no change within error.**

Our results suggest that material may have been deposited on areas such as Smooth Plains Site 5 (Fig. 3), while areas such as smooth plains examples in the interior of the Imhotep region (Type-example and Site 1, Fig. 3) may be removing their dusty upper layers revealing fresher, ice-rich material. However, the spectral changes, and thus material transport, are not consistent within a singular morphology, nor within a singular region. Spectral changes in the smooth plains morphology vary even though the sites chosen are in similar locations. The variation in spectral changes both within each morphology and previously defined regions supports the interpretation that the processes evolving the surface of 67P act on local (~100 m) scales.

References: [**1**] Birch, et al., (2017), S50-S67. [**2**] El-Maary, et al, (2019) *Space Science Reviews*, 215(4), 36. [**3**] Thomas, et al., (2015), *Science*, S*47*(6220), aaa0440.[**4**] Hapke, (2012), CUP.[**5**] Cappacioni, et.al., (2015) *Science*, *347* (6220). **[6]** Fornasier, et al., (2015) *AAS*, *583*, A30 **[7]** Acton, et.al., (2018), Planetary and Space Sciences, 150, 9-12. **[8]** Oklay, et al (2016) *MN RAS* 426